Structural and quantitative analysis of nitrided stainless steel coatings deposited by dc-magnetron sputtering.

Terwagne, Guy; Colaux, Julie; Collins, George; Bodart, Franz

Published in:
Thin Solid Films

Publication date:
2000

Document Version
Publisher's PDF, also known as Version of record

ELSEVIER

Thin Solid Films 377–378 (2000) 441–446

thin solid films

www.elsevier.com/locate/tsf

Structural and quantitative analysis of nitrided stainless steel coatings deposited by dc-magnetron sputtering

G. Terwagne[a,*], J. Colaux[a], G.A. Collins[b], F. Bodart[a]

[a] *Laboratoire d'Analyses par Réactions Nucléaires, Facultés Universitaires Notre-Dame de la Paix, 61, rue de Buxelles-B-5000, Namur, Belgium*

[b] *Australian Nuclear Science and Technology Organisation, Lucas Heights PMB 1, Menai, Australia*

Abstract

Stainless steel coatings were deposited at a low temperature on low-carbon steel and mono-crystalline silicon substrates by dc-magnetron sputtering in a reactive atmosphere of nitrogen at room temperature. The total mass flow of argon and nitrogen was kept constant (20 sccm) for all depositions and the nitrogen mass flow varied between 0 and 10 sccm with increments of 1 sccm, while the argon mass flow was decreased by the same amount. The elemental composition of the coatings and their deposition rate were studied by Rutherford backscattering spectroscopy (RBS), by X-ray emission induced by charge particles (PIXE), and by nuclear reaction analysis (NRA). The nitrogen content was found to increase with increasing mass flow up to a saturation value of 40 at.%. A structural analysis by means of conversion electron Mössbauer spectroscopy (CEMS) and grazing incidence X-ray diffraction (GXRD) was also performed. The results indicated the presence of the so-called *S*-phase, probably due to nitrogen in solid solution at interstitial sites in the austenite lattice. The lattice expanded as the nitrogen mass flow increased. This phase is particularly interesting for industrial applications because it increased the resistance to wear without compromising the corrosion resistance of the steel.

Keywords: PVD; Magnetron sputtering; Stainless steel; Nitrogen

1. Introduction

Austenitic stainless steels are well known for their corrosion resistant qualities but their performance is limited by their poor wear resistance. Nitriding of these steels can be performed by several techniques, such as conventional ion implantation [1–6], pulsed plasma nitriding [7] and plasma immersion ion implantation (PI^3) [8]. As long as the treatment temperature is kept below a critical value of approximately 450°C, the wear resistance can be improved without compromising the corrosion performance. At these lower temperatures, nitrogen remains in solid solution, producing a phase that has been variously called the 'S-phase' [9], 'expanded austenite' [10,11] or γ_N phase [4–6].

Magnetron sputtering offers new possibilities and more flexibility for producing coatings on various substrates at low temperatures. While coatings sputtered from austenitic stainless steel targets at a low temperature usually form a ferritic bcc structure [12], the addition of nitrogen to the sputtering gas results in a nitrogen-supersaturated fcc phase with improved wear resistance and higher corrosion resistance [13–15]. These coatings, whose properties and structure are similar to the 'S-phase' produced by nitriding, can be produced by dc-magnetron sputtering using stainless steel targets — a more convenient option than using expensive chromium targets to produce CrN coatings.

The purpose of this paper was to present a detailed

* Corresponding author. Tel.: +32-81-72-54-78; fax: +32-81-72-54-74.

E-mail address: guy.terwagne@fundp.ac.be (G. Terwagne).

0040-6090/00/$ - see front matter
PII: S0040-6090(00)01279-7

analysis (elemental and structural composition) of coatings sputtered from a stainless steel (AISI 303) target in nitrogen/argon gas mixtures. Elemental composition analysis was realized by nuclear reactions analysis (NRA), X-ray emission induced by charge particles (PIXE) and Rutherford backscattering spectroscopy (RBS), whereas structural analysis was performed by means of conversion electron Mössbauer spectroscopy (CEMS) and grazing X-ray diffraction (GXRD).

2. Sample preparation

The coatings were deposited using an unbalanced dc-magnetron sputtering system placed in a small chamber of 0.05 m^3 equipped with a 280-l/s turbomolecular pump which provided a base pressure of 10^{-5} Pa. A 50-mm diameter AISI-303 (composition in wt.% — Fe: 70%, Cr: 18%, Ni: 9%, Mn: 2%, and Si:1%) disk target was placed just above the magnets with a good thermal contact to the holder in order to cool the magnetic material with water during deposition. The source to sample holder distance was 150 mm and a chimney was placed on the top of the target to prevent contamination of the whole chamber. A shutter was placed between the top of the chimney and the sample holder in order to avoid deposition during target cleaning for 5 min before each deposition.

Two sets of substrates were used in this study:

1. Si (100) wafers to measure the deposition rates and the elemental analysis of the coatings; and
2. low-carbon steel for the elemental and structural analysis.

Substrates were cut into 20×20 mm square coupons and cleaned in an ultrasonic bath with pentane before loading into the chamber. Prior to each deposition, the substrates (which were grounded) were etched for 2 min in order to remove oxide from the steel surface and to enhance coating adhesion.

Depositions were made at room temperature in the same conditions for both sets of substrates. The magnetron power was set to 100 W during deposition and the voltage applied to the sputter target was approximately -400 V. Although the substrate was heated by electron and ion bombardment, the temperature was measured below 100°C during deposition with a thermocouple placed at the rear of the specimen. The coatings were reactively deposited for 20 min with various Ar/N_2 gas mixtures, which gave a thickness of approximately 400 nm. The proportion of N_2 in the sputter gas was varied by changing the N_2 flow rate with a compensating adjustment of the Ar flow rate, such that the total gas flow rate remained constant at 20 sccm. These flows correspond to a total pressure of 0.27 Pa measured with a baratron gauge placed in the deposition chamber.

3. Coating characterization

3.1. Elemental analysis

Nuclear elemental analyses were performed at LARN with ALTAÏS, the new 2-MV Tandetron accelerator. The thickness and composition of the coatings were measured by Rutherford backscattering spectroscopy (RBS) and particle-induced X-ray emission (PIXE) techniques with 2 MeV incident α particles. These measurements were made on the coatings on silicon substrates to avoid interfering signals from the substrate. The scattered particles were detected in a passivated implanted planar silicon detector (PIPS) at 175° relative to the incident beam. By fitting the experimental spectrum, it was possible to obtain the thickness of the coating. The deposition rates were then calculated and are presented in Fig. 1. The Si(Li) detector placed at 135° relative to incident beam recorded X-rays emitted from the sample during RBS measurements. The relative amounts of Cr, Fe, Ni and Mn measured by the PIXE technique are reported in Table 1.

Nuclear reaction analysis (NRA) was used to measure the nitrogen concentration using $^{14}N(\alpha,p)^{17}O$ at 4.8 MeV. A typical particle spectrum is shown in Fig. 2. Although endoenergetic ($Q = -1.191$ MeV), this nuclear reaction was suitable for nitrogen analysis because it showed a constant cross section (5 mb/sr) at 90° for incident energies ranging between 4.6 and 4.8 MeV [16]. A 24.4-μm mylar absorber was placed in front of the particle detector to avoid elastic scattered particles in the PIPS detector. The nitrogen concentrations are also reported in Table 1.

Table 1
Relative amount of Fe, Cr, Ni and Mn measured for different coatings. Argon and nitrogen flow percentages are relative to the total flux in the deposition chamber

Ar flow (%)	N_2 flow (%)	[Fe] (at.%)	[Cr] (at.%)	[Ni] (at.%)	[Mn] (at.%)	[N] (at.%)
100	0	70.4	19.2	8.5	2.0	0.0
95	5	62.0	16.8	7.5	1.8	11.9
90	10	55.2	15.0	6.7	1.6	17.0
85	15	51.5	13.9	6.3	1.5	26.8
80	20	48.0	13.0	5.8	1.4	31.7
75	25	45.3	12.3	5.5	1.3	35.6
70	30	43.3	11.7	5.3	1.3	38.4
65	35	43.3	11.7	5.3	1.3	38.4
60	40	40.8	11.0	5.0	1.2	42.0
55	45	37.8	10.2	4.6	1.1	46.2
50	50	37.6	10.2	4.6	1.1	46.5

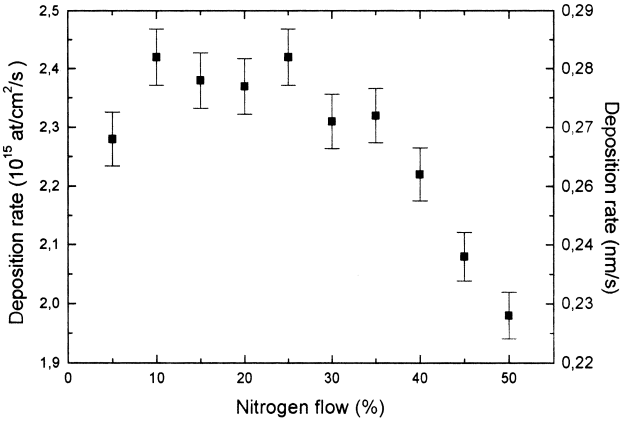

Fig. 1. Deposition rates measured by RBS technique on the coatings on silicon substrates as a function of nitrogen flow.

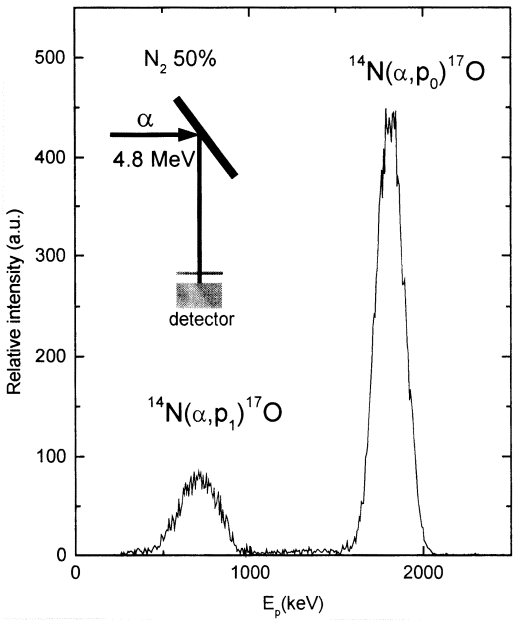

Fig. 2. Experimental NRA spectrum measured with 4.8 MeV α-particles detected at 90° for a typical stainless steel coating deposited by unbalanced dc-magnetron sputtering on a low carbon steel substrate.

3.2. Structural analysis

Conversion electron Mössbauer spectroscopy (CEMS) was used to determine the different phases formed after deposition of the nitrogen-rich stainless steel coatings on the low carbon steel substrates. As is well known, CEMS is most sensitive to the top 0.1 μm (nearly 80% of conversion electrons come from this depth), even though there is some contribution to the signal from depths up to ~ 0.3 μm, but with decreasing efficiency [17]. The Mössbauer measurements were made at room temperature using a ^{57}Co source in a rhodium matrix with an initial activity of 50 mCi. The specimen of interest was placed in gas flow proportional counter where the 7.3-keV conversion electrons resulting from recoilless resonant absorption by ^{57}Fe nuclei within the specimen were detected. The velocity of the Mössbauer spectrometer was calibrated by recording a reference spectrum of an α-Fe phase present in metallic iron. The Mössbauer spectra recorded on each sample are presented in Fig. 3. On each Mössbauer spectrum (Fig. 3b–l) we can observe the sextet due to α-Fe present in the low carbon steel (same sextet as in Fig. 3a). A few ferromagnetic compo-

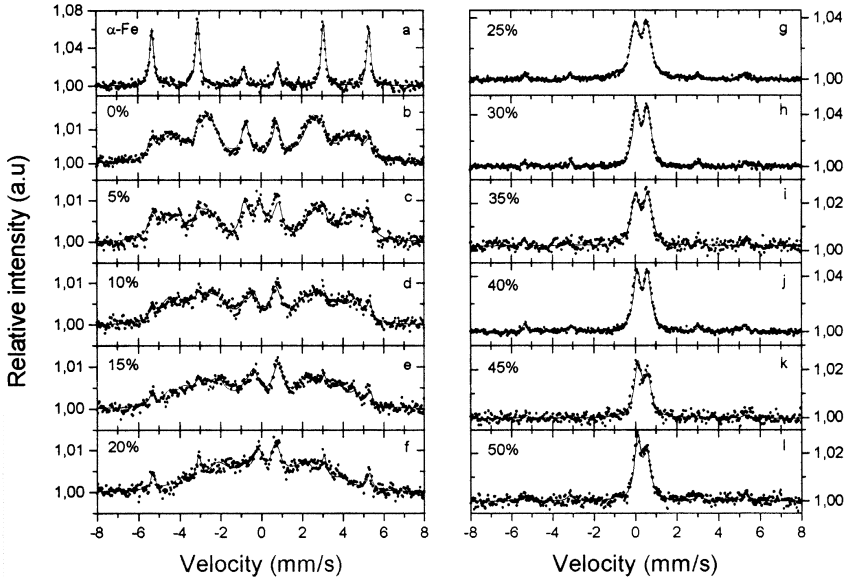

Fig. 3. Mössbauer spectra obtained by CEMS technique on: (a) metallic α-Fe iron; and (b)–(l) stainless steel coating deposited by dc-magnetron sputtering on a low carbon steel substrate in different flows reactive gas mixing atmosphere of argon and nitrogen. The relative amount of nitrogen is indicated on the left upper corner of each figure.

nents were also observed for low N_2 flows ($< 25\%$) and a paramagnetic doublet was observed for higher N_2 flows.

Grazing incidence XRD patterns were obtained from the coatings on the low carbon steel substrates with a Siemens D500 diffractometer using CoKα radiation ($\lambda = 1.789$ Å) with a post-specimen monochromator acting in the parallel mode. The scans were performed at an incidence angle $\alpha = 1°$ over Bragg angles from $2\theta = 30°$ to $2\theta = 80°$, counting for 30 s at 0.05° intervals. The grazing incidence XRD patterns had a substantial background, particularly at lower Bragg angles. There was also a component from the sample holder. With the broad peaks produced in the sputtered coatings, it was difficult to use standard background subtraction routines. As an alternative, the background was calculated from an uncoated sample and subtracted from the scans obtained from the coated samples. The results are shown in Fig. 4a,b.

The small unidentified peaks in the GXRD patterns at $2\theta = 31.8°$, 41.8°, 48.1° and 63.8° were present in the diffraction pattern obtained from an empty sample holder, although the last three also corresponded to peaks from Fe_2O_3. No additional peaks were visible from the coating deposited in pure argon. The 5% N_2 flow coating had a peak at $2\theta = 51.3°$ which was close to the position of the (111) γ-austenite peak (51.05°). At higher a nitrogen content in the gas flow, this peak was replaced by a broad peak, labeled *S* [14] in Fig. 4, which moved to lower Bragg angles and broadened as the nitrogen content in the gas flow was increased. At 50% N_2 flow, the peak eventually disappeared although a new peak at $2\theta = 41°$ appeared. Another broad peak appeared at $2\theta = 68°$ in the sample deposited with 45% N_2 flow which moved up to $2\theta = 69°$ in the sample made with 50% N_2 flow.

4. Results and discussion

Fig. 5 shows the evolution of nitrogen concentration in the coatings corresponding to different nitrogen flows. The results obtained by NRA and RBS techniques showed a remarkable agreement. The total amount of nitrogen was found to be proportional to the nitrogen flow until this reached 25% of the total flow. At higher flow, a maximum nitrogen content of approximately 40% was measured. These results were very similar to those reported by other authors [13,15].

Combining PIXE and RBS analysis, we could observe that the relative iron, chromium and nickel compositions of all nitrogen-containing coatings were within the specifications of AISI 303 stainless steel. As the nitrogen content of the coating increased, these elements decreased proportionally, indicating that iron, chromium and nickel atoms were transferred from the target to the sample in constant proportions. This be-

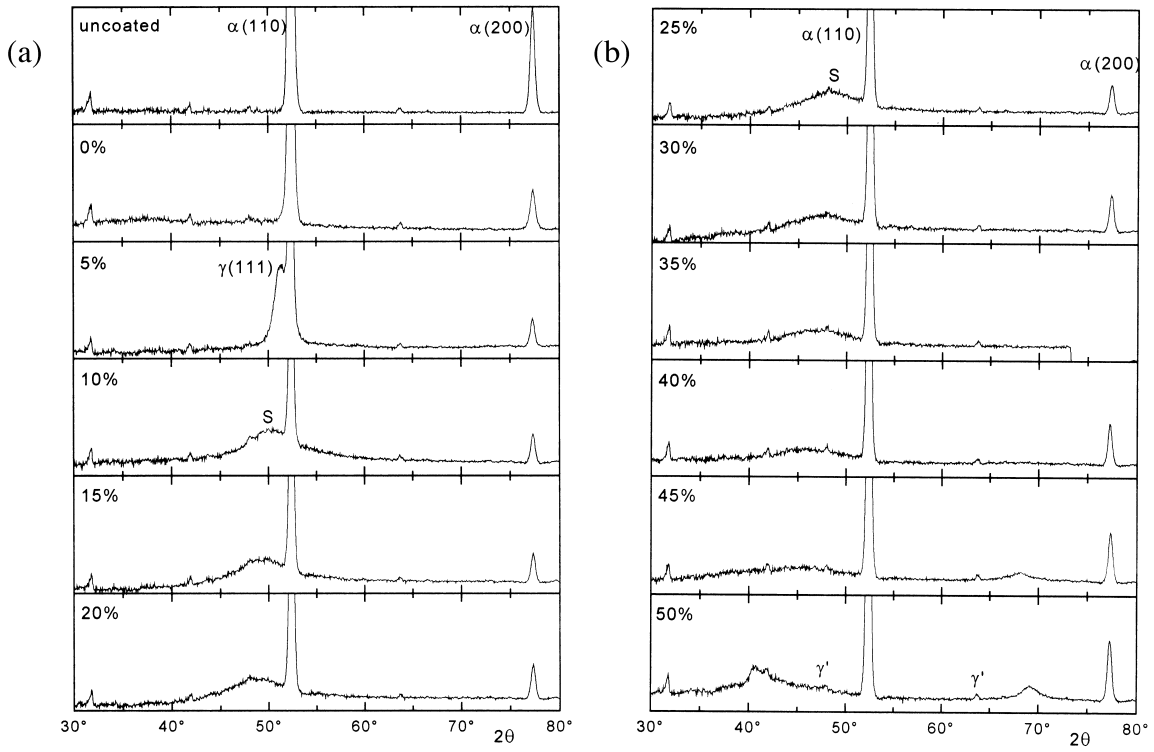

Fig. 4. GXRD spectra observed at $\alpha = 1°$ for the stainless steel coatings deposited by DC-magnetron sputtering on low carbon steel substrates in a reactive argon and nitrogen atmosphere: (a) for the uncoated sample and low nitrogen flows; and (b) for high nitrogen flows.

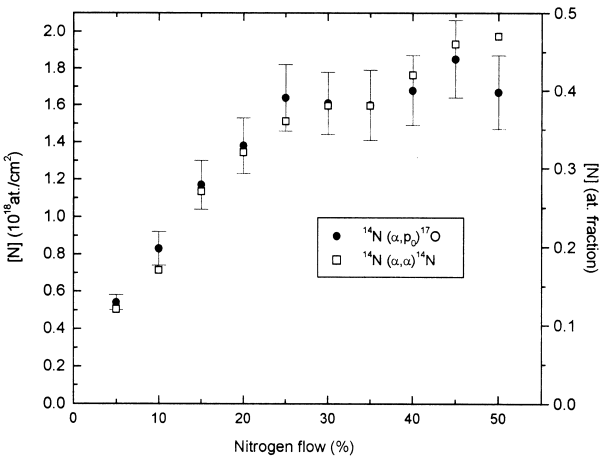

Fig. 5. Nitrogen concentrations vs. nitrogen flow measured by NRA and RBS techniques for the stainless steel coatings deposited by dc-magnetron sputtering on low carbon steel substrates in a reactive argon and nitrogen atmosphere.

havior has also been reported by Shedden et al. [15]. This was due to the sputter yield amplification effect. The differences in partial sputtering yield for nickel, chromium and iron (1.05, 0.96 and 0.87, respectively, for 400-eV Ar ions [18]) resulted in target surface enrichment of the slowest sputtering element. The target quickly reached a steady state condition, even though the target surface chemistry was altered.

We have presented in Fig. 1 the deposition rate as a function of nitrogen flow. Below 25% of N_2, the deposition rate remained constant, while it dropped drastically for higher flows. For low nitrogen flow (below 25%), the constant deposition rate could be related to the nitrogen concentration in the coating (Fig. 5) which increased linearly. This means that we operated in a metallic mode of deposition — the sample, the target and the chimney consumed all nitrogen atoms introduced in the chamber. Above 25% nitrogen flow, the AISI-303 target was poisoned with nitrogen and the sputtering yields of target elements were reduced. The deposition rates decreased and the coatings were saturated with nitrogen. It seems that this effect was due to a transition between metallic to compound modes of deposition, which was produced when the cathode was polluted with nitrogen.

Mössbauer spectra recorded on the low carbon steel substrate (α-Fe) and stainless steel coatings produced without nitrogen are presented in Fig. 3. A single magnetic internal field was observed on α-Fe (Fig. 3a) while this magnetic field was modified when the near-neighbor atom of iron was an element from AISI 303, such as chromium or nickel [19]. We can observe in Fig. 3b,c a broad magnetic component which could be decomposed with three different sextets. Hyperfine parameters, such as internal magnetic field, were reduced for the coating performed in a pure argon atmosphere. The same behavior was also observed for the coatings performed with nitrogen flow below 20% of the total flow (Fig. 3c–f). When the nitrogen concentration was increased, the internal magnetic field was decreased and the coatings suddenly showed a paramagnetic behavior for nitrogen flows above 25% (Fig. 3g–l). This effect has also been observed by Bobo et al. [20] on iron nitride films obtained by argon–nitrogen reactive radio-frequency sputtering. At 5% nitrogen flow (Fig. 3c), we also observed a single peak at approximately zero velocity, which was due to an austenitic γ-Fe phase. GXRD confirms this result — a well-defined austenitic γ(111) peak appeared for the coating with a nitrogen flow of 5% (Fig. 4a). For the higher flows of nitrogen (45% and 50%), the Mössbauer spectra showed an asymmetric doublet which was due to the presence of a single peak at velocity 0.12 mm/s. This peak could be related to the GXRD results. Indeed, for high flow of nitrogen, a broad peak, which has not yet been attributed, appeared near an angle of $2\theta = 68°$ (Fig. 4b).

Gaussian peak fitting was used to quantify the *S*-phase peak in Fig. 4a,b. Although the very large (110) α-Fe peak was excluded from the fitting process, its remnant required a second Gaussian to accurately fit the data. The *d*-spacings calculated from the peak position are plotted in Fig. 6 which shows a steady 'expansion' as the nitrogen content in the gas flow was increased, similar to that observed by others. The data from Dahm and Dearnley [14] are also plotted in Fig. 6 and showed a remarkable similarity to the present data, although the thickness of their coatings were thicker than the present one.

5. Conclusions

Nitrided stainless steel coatings (AISI-303 cathode) deposited at room temperature by dc-magnetron sputtering on low carbon steel substrates show two modes

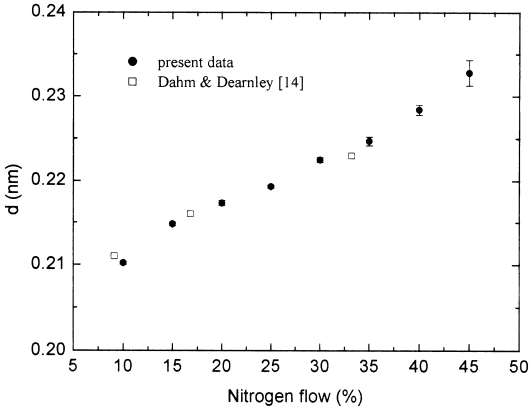

Fig. 6. *d*-Spacings vs. nitrogen flows calculated from fitted peak positions.

of deposition. At low N_2 flows, the metallic regime of deposition is predominant and high deposition rates are observed. A nitrogen '*S*-phase' is formed in the deposited coating and lattice expansion is observed, which confirms the results obtained by Dahm and Dearnley [14]. The nitrided layers contain a ferromagnetic structure. At higher flows of nitrogen ($>25\%$), a compound mode of deposition is observed and the deposition rates decrease rapidly. At these flows, a maximum concentration of approximately 40 at.% of nitrogen was measured in these coatings, which exhibited paramagnetic properties. Future investigations will be performed on those samples, as for example, CEMS performed at low temperatures, in order to measure the Curie temperature of the coating.

References

[1] G. Wagner, T. Louis, R. Leutenecker, U. Gonser, Hyperfine interactions 46 (1989) 501.
[2] D.L. Williamson, O. Orturk, S. Glich, R. Wei, P.J. Wilbur, Nucl. Instr. Methods, B59/60 (1991).
[3] Th. Briglia, G. Terwagne, F. Bodart, C. Qwaeyhaegens, J. D'Haen, L.M. Stals, Surf. Coat. Technol. 80 (1996) 105.
[4] D.L. Williamson, J.A. Davies, P.J. Wilbur, Surf. Coat. Technol. 103–104 (1998) 178.
[5] R. Wei, Surf. Coat. Technol. 83 (1996) 218.
[6] O. Oztürk, D.L. Williamson, J. Appl. Phys. 77 (1995) 3839.
[7] E. Menthe, K.T. Rie, J.W. Schultze, S. Simson, Surf. Coat. Technol. 74–75 (1995) 412.
[8] G.A. Collins, R. Hutchings, J. Tendys, Mater. Sci. Eng. A139 (1991) 171.
[9] K. Ichii, K. Fujimura, T. Takase, Technol. Rep. Kansai Univ. 27 (1986) 135.
[10] R.G. Vardiman, I.L. Singer, Mater. Lett. 2 (1983) 150.
[11] M.P. Fewell, D.R.G. Michell, J.M. Priest, K.T. Short, G.A. Collins, to be published in Surf. Coat. Technol.
[12] S.D. Dahlgren, Metall. Trans. 1 (1970) 3095.
[13] A. Bourjot, M. Foos, C. Frantz, Surf. Coat. Technol. 43–44 (1990) 533.
[14] K.L. Dahm, P.A. Dearnley, Surf. Eng. 12 (1996) 61.
[15] B.A. Shedden, F.N. Kaul, M. Samandi, B. Window, Surf. Coat. Technol. 97 (1997) 102.
[16] G. Terwagne, to be published.
[17] D.L. Williamson, F.M. Kustas, M.S. Misra, J. Appl. Phys. 60 (1986) 1493.
[18] Handbook of Vacuum Science and Technology, in: D.M. Hoffman, (Eds.), Bawa Singh, John H. Thomas, III, 611.
[19] I. Vincze, I.A. Campbell, J. Phys. F Met. Phys. 3 (1973) 647.
[20] J.F. Bobo, H. Chatbi, M. Vergnat, L. Hennet, O. Lenoble, Ph. Bauer, M. Piecuch, J. Appl. Phys. 77 (1995) 5309.